Computational Fluid Dynamics of Ionic Wind in a Corona Device in Electrophotography-(1)

Kazuhiro Mori

Reliability Engineering of Technology, Development Management, Development & Manufacturing Group, Fuji Xerox Co., Ltd., Ebina-shi, Kanagawa, JAPAN

Hideki Okamoto and Nobuyuki Hirooka

Key Technologies Development, Technology & Development, Development & Manufacturing Group, Fuji Xerox Co., Ltd., Nakai-machi, Ashigarakami-gun, Kanagawa, JAPAN

Ionic wind occurs with corona discharge. Knowledge of the ionic wind in a machine is necessary for a measure of the degradation of the image that originates from the generation products on corona discharge. We investigate the characteristics of the ionic wind in the neighborhood of a corona device through Computational Fluid Dynamics to better understand this phenomenon. Various flow characteristics have been found. A λ-shaped flow appears on a cross section in the fan-off case. Several vortices are induced by the λ-shaped flow. Static pressure descends along the wire. We also find three-dimensional features. There is a countercurrent at both ends of the corona device. Momentum is axially transported. Our numerical calculations correlate well with our experimental results by Particle Image Velocimetry (PIV) and smokes. The λ-shaped flow appears also on a cross section in the fan-on case, while the flow rate of the whole system is hardly changed. The ionic wind locally has an influence on the flow field in the neighborhood of the corona device.

Journal of Imaging Science and Technology 48: 465–472 (2004)

Introduction

Corona discharge is used for charging in electrophotography.[1] Although charging rollers are often used to reduce the ozone concentration, they damage photoreceptors more severely than corona devices. Accordingly, corona devices are still used in high-speed machines. However, corona devices cause ionic wind. Ionic wind occurs as a result of the Coulomb force exerted on ions, and collisions of ions and neutral molecules of gas.[2] Ions collide with the molecules of air, and impart momentum to the air. The ionic wind transports oxidation products, which cause the degradation of the image and environmental problems. Therefore, knowledge of the flow field in the neighborhood of corona devices is necessary, so that, the ionic wind can be considered in designing machines including corona devices. Although manifestations of the ionic wind have been observed in open space, it is impossible to measure accurately the flow field in a confined space. Physical phenomena occurring in confined spaces have generally been difficult to quantify,[3] and moreover, the influence of the electric field is strong. Measurement by a Pitot tube or a hot-wire anemometer is difficult. Therefore, we numerically predicted the characteristics of the ionic wind in a confined space.

Many investigations about corona discharge including the ionic wind[2,4–9] have been conducted. Yabe and co-workers[2] analyzed the ionic wind from an electrohydrodynamical approach. Léger and co-workers[5] analyzed ability of a dc electrical discharge to control low-velocity airflow along a flat plate. Yamamoto and co-workers[6] investigated three-dimensional electrhydrodynamics in the wire-duct electrostatic precipitator. In electrophotography, Nashimoto[7] carried out a parametric experiment on ozone generation on corotrons to investigate effects of discharge wire and shield materials, wire diameter, and the difference of positive and negative corona. Since understanding the degradation phenomena of the corona wire is significant, Hoshino and Hayashi[8] investigated effect of airflow and Isopar™ vapor on corona discharge. Okamoto and Mori[9] recently reported the ionic wind in a corona device with consideration of the rotation of the photoreceptor.

We are able to comprehend the basic behavior of the ionic wind in open space. A λ-shaped flow appears on a cross section. A countercurrent occurs at the edge of the corona device and momentum is axially transported. However, a fan is usually working during corona discharge. The ionic wind in the fan-on case has never been studied. Knowledge of the ionic wind in a machine is necessary for a measure of the degradation of the im-

Original manuscript received February 2, 2004

Kazuhiro.Mori@fujixerox.co.jp

TABLE I. Parameter for a P-Q Diagram of a Fan

P(Pa)	Q (m^3/min)
500	0
0.0	2.25

TABLE II. Geometrical Parameters for a Corona Device and a Photoreceptor

Width of corona device (m)	2.8×10^{-2}
Height of corona device (m)	1.7×10^{-2}
Length of corona device (m)	3.9×10^{-1}
Width of ventilation slit (m)	7.0×10^{-3}
Length of ventilation slit (m)	3.2×10^{-1}
Diameter of corona wire (m)	3.0×10^{-5}
Diameter of photoreceptor (m)	8.4×10^{-2}
Space between grid and photoreceptor (m)	1.2×10^{-3}

age that originates from corona discharge generation products. Therefore, in this study we investigate the ionic wind phenomenon in a machine in the fan-on case. We can numerically predict the steady flow field and contours of the concentration of ozone.

In this article, we synthetically report the basic characteristics of the ionic wind. The following section discusses the analysis model and numerical conditions. The third section describes the electric field and coupled calculations. The body force due to the electric field is first calculated with the two-dimensional corona discharge simulation. Next, we use a computer program FLUENT Ver. 6.1.18 (FLUENT Inc., Lebanon, NH, USA) to calculate the three-dimensional flow field. The fourth section briefly describes phenomenon in the fan-off case. Velocity vectors by Particle Image Velocimetry (PIV) are also shown. Our numerical calculations correlate well with our experimental results. The fifth section has velocity vectors, contours of static pressure in a middle plane and marker particle path lines in the fan-on case. The sixth section describes the simplified concentration analysis. We also show contours of the concentration of ozone in the middle plane and contours of the concentration of ozone on the surface of the photoreceptor. We have found various flow characteristics. Finally, we summarize the basic characteristics of the ionic wind.

Analysis Model and Conditions for Numerical Calculations

Figure 1(a) shows an analysis model with two inlets and an outlet. This model has about 5 million tetra cells. The front of the model is called the outboard side and the back of the model is called the inboard side, respectively. The analysis model consists of a rectangular prism, 660 mm long, with cross-sectional dimensions of 435 mm × 792 mm. Airflow which leads ozone to the absorption filter to remove ozone is necessary. Figure 1(b) shows an airflow system. The gray level of the marker particle path lines indicate velocity magnitude (m/s). Markers are massless. We think of a configuration such as an airflow system with ducts, where air is driven air to the lower part by a fan. The duct is 588 mm in length, 425 mm in width and 653 mm in height. The pressure is prescribed as 0 at the inlet and outlet boundaries. Pressure means static gauge pressure. The other surfaces are no slip walls. We monitored the flow rate at the ventilation slit of the corona device with the residuals. A fan exhausts air below. The fan is considered to be infinitely thin, and the discontinuous pressure rise across it is specified as a function of the velocity through the fan. The relationship is defined by a piecewise linear one, the so-called *P*-*Q* diagram. Here, *P* is the pressure rise across the fan and *Q* is the flow rate through the fan. Since the fan is considered to be infinitely thin, it must be modeled as the surface between cells. By the balance of the *P*-*Q* diagram and the mechanical impedance, we can determine a pressure rise on the fan and the system flow rate. The *P*-*Q* diagram is summarized in Table I. The flow rate of 2.25 m^3/min is equivalent to the average velocity of 15.9 m/s across the fan.

Since we investigate the basic characteristics of the ionic wind in this article, our studies have focused on the flow field in the neighborhood of the corona device. Figure 1(c) shows the neighborhood of the corona device and the photoreceptor. In addition, Figure 1(d) shows the corona device and the photoreceptor. The corona device is depicted as a rectangular solid attached to the cylindrical photoreceptor. The corona device has insulator blocks on both ends to stretch a wire electrode. There is a slit for ventilation on the ceiling of the shield electrode. A cross section in the neighborhood of the corona device is shown in Fig. 1(e). The wire electrode is stretched in the center of the metal shield electrode. The axial direction of the wire is the z-direction. A grid electrode is set between the wire electrode and photoreceptor to help with uniform charging. The existence of the wire is negligible since the diameter of the wire is small compared with the flow field. The grid is also neglected since the number of openings is large. Table II shows geometrical parameters for the corona device and the photoreceptor. The photoreceptor rotates clockwise at 0.22 m/s.

Electric Field and Coupled Calculations

The ionic wind is a complex phenomenon designed by multiple parameters. The electric field, flow field and temperature field mutually affect one another. Since the electrostatic force to the air is dominant, other effects are negligible in this analysis. Electrostatic force is calculated from the distribution of the electric field and charge density. These distributions are obtained by solving the Poisson equation

$$\frac{\partial\left(\varepsilon_{ij}\boldsymbol{E}_j\right)}{\partial x_i} = \rho_e, \tag{1}$$

and the charge conservation equation

$$\frac{\partial \rho_e}{\partial t} + \frac{\partial\left(\mu_e \rho_e \boldsymbol{E}_j\right)}{\partial x_i} = 0, \tag{2}$$

where ε_{ij} is the permittivity, E_i (i = 1,2,3) represent the Cartesian components of the electric field $\boldsymbol{E}$, ρ_e is the charge density, μ_e is ion mobility and x_i (i = 1,2,3) represent the Cartesian coordinates. Here, we adopted the Einstein convention that whenever the index appeared twice in any term, we implied the summation over the range of that index. Equations (1) and (2) are solved by the finite difference method. Charge and electric potential terms are coupled in Eqs. (1) and (2). By time marching, electric potential and charge distribution are alternately calculated until they reach a steady state. Then, we used the successive over-relaxation (SOR)

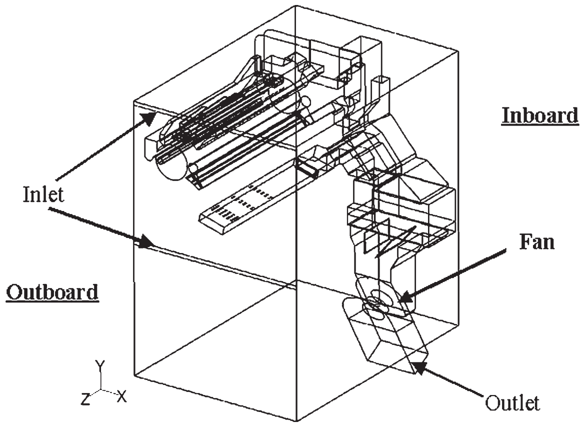

Figure 1(a). An analysis model

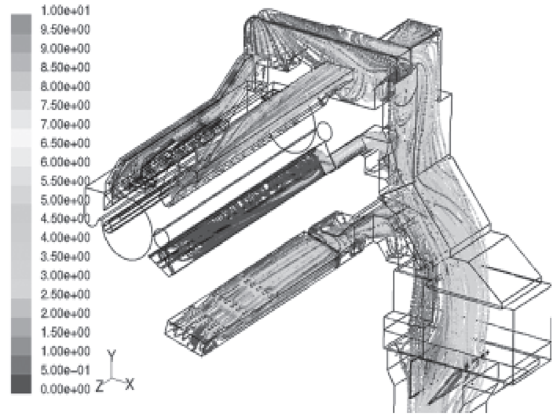

Figure 1(b). An airflow system

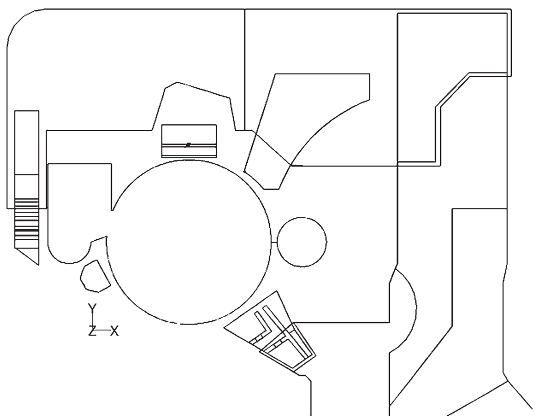

Figure 1(c). A cross section diagram in the neighborhood of the corona device

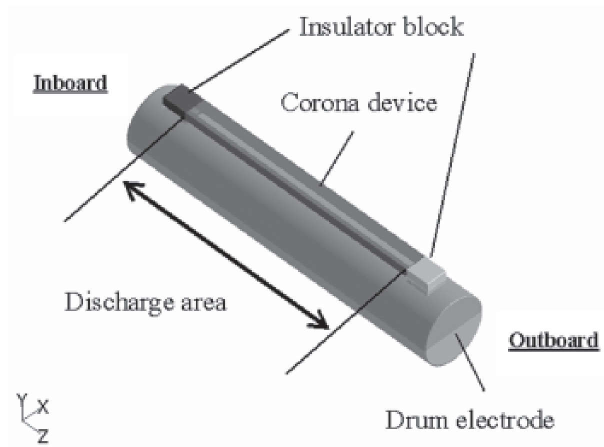

Figure 1(d). The corona device and the photoreceptor

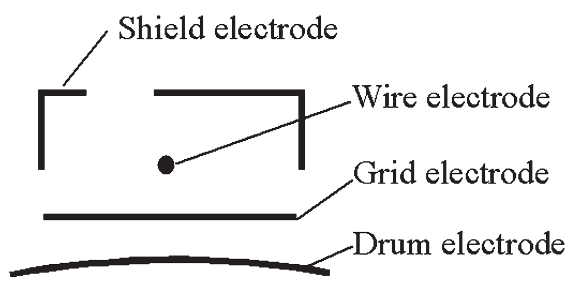

Figure 1(e). A cross section diagram of the corona device

method as the matrix solver. The electric current produced by corona discharge is given by Sarma's assumption.[10] The charge density around the wire is set to keep the intensity of the electric field at threshold strength on its surface. Calculation of the electric field is done on the cross section of the corona device, since the configuration of the corona device is uniform along the corona wire. Distributions of electric potential and charge density are shown in Figs. 2(a) and 2(b). Effect of charging on the photoreceptor is small inside the corona device. The charge density between the wire and the photoreceptor is high. The number of charges outside the shield case are small. In this study, we first calculated the body force with the two-dimensional corona discharge simulation. Next, FLUENT can numerically predict the flow field by considering the body force as the volumetric source term of momentum.

FLUENT numerically solves Navier–Stokes equations:

$$\frac{\partial \rho}{\partial t} + \frac{\partial (\rho u_j)}{\partial x_i} = 0, \tag{3}$$

$$\frac{\partial (\rho u_i)}{\partial t} + \frac{\partial (\rho u_i u_j)}{\partial x_i} = -\frac{\partial \rho}{\partial x_i} + \frac{\partial}{\partial x_i}\left(\mu \frac{\partial u_i}{\partial x_i}\right) + F_i, \tag{4}$$

$$F_i = \rho_e E_i, \tag{5}$$

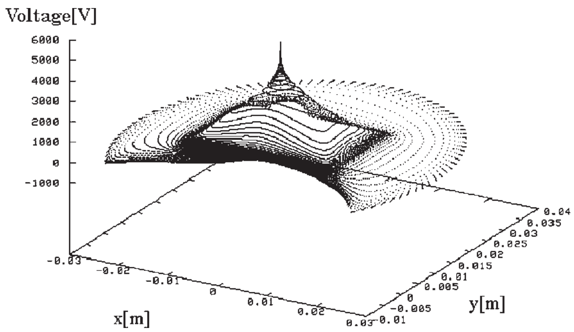

Figure 2(a). Distribution of electric potential

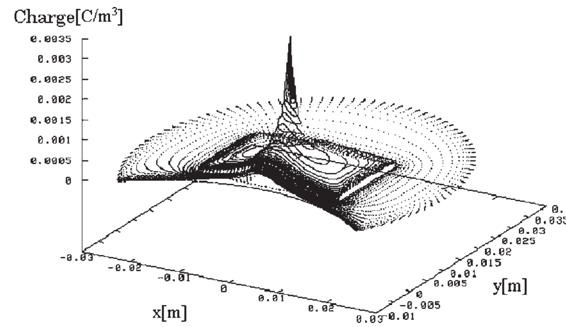

Figure 2(b). Distribution of charge density

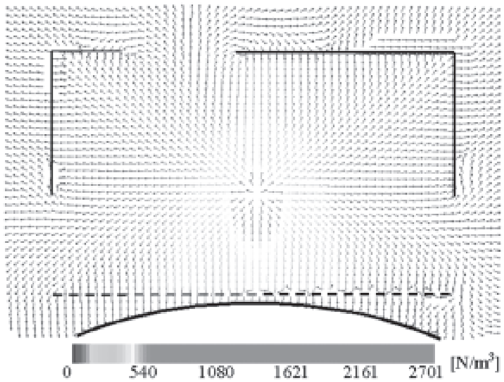

Figure 2(c). Distribution of body force

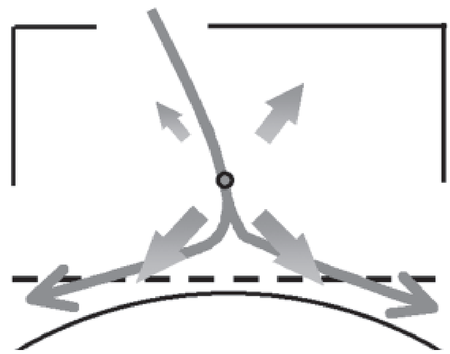

Figure 2(d). Schematic distribution of body force

where ρ is the fluid density, p is the static pressure, u_i (i = 1,2,3) represent the Cartesian components of velocity u, F_i (i= 1,2,3) represent the Cartesian components of the body force derived from the ionic wind and μ is the molecular viscosity of the fluid. We used constant values $\rho = 1.204$ kg/m^3 and $\mu = 1.808 \times 10^{-5}$ kg/m·s. It is reasonable to assume the fluid is incompressible for this problem. The distribution of the body force obtained by Eq. (5) is shown in Fig. 2(c).

The calculation grids around the wire electrode are very fine, because the electric potential and charge distribution change drastically there. The grid spacing is set to the minimum value 10^{-6} m in the wire vicinity. Since the grids for airflow simulation are different, the body force at the grid points are calculated by linear interpolation from the results of the electric field simulation. The body force extends radially from the wire. The body force is stronger between the wire and the photoreceptor. In contrast, the body force is weaker at the upper ventilation slit. The schematic distribution of the body force is shown in Fig. 2(d). By using the User Defined Function[11] to capture the body force as the volumetric source term, FLUENT calculates the three-dimensional flow field.

Ionic Wind Phenomenon in the Fan-off Case

Okamoto and Mori[9] recently reported the ionic wind in open space with the considering the rotation of the photoreceptor. It was shown that λ-shaped flow appears on a cross section. We could comprehend that the λ-shaped flow is derived from the schematic distribution of the body force, and we found that several vortices are induced by this λ-shaped flow.

By using the analysis model in Fig. 1(a), we show the behavior of the ionic wind in the fan-off case. Airflow is mainly induced by corona discharge. Figure 3(a) shows velocity vectors in the neighborhood of the corona device in a middle plane. The grayscale indicates velocity magnitude (m/s).

Itoh and co-workers[4] examined laminar flow around a wire electrode, induced by corona discharge in a system of wire and plate electrodes, to give some information for the self-excited lateral oscillation of the wire electrode. Since the wire was negligible, the Reynolds number in large scale space, R_E = 5000 was calculated. A reference velocity was defined by balancing the convection term and the Coulomb force, and a reference length was defined by setting the distance between the wire and the plate. They also investigated the fluid field around the wire by modeling the wire for the same phenomenon. The Reynolds number R_E is sufficiently small, and the flow field is laminar. We calculated the Reynolds number in large scale space, R_E = 2700 for our model in the fan-off case. We defined a reference velocity U = 2 m/s and a reference length L = 0.02 m. It is reasonable to assume that the flow field is laminar in the fan-off case.

Figure 3(b) shows contours of static pressure in the middle plane. These contours are colored by static pressure (Pa). Static pressure rises in the region where the ionic wind collides with the photoreceptor. In contrast, static pressure decreases along the wire. Figure 3(c) shows marker particle path lines with grayscale indicating velocity magnitude of the flow field (m/s). A flow rate through the ventilation slit is 0.05445 m^3/min. Figure 3(d) shows velocity vectors at the end of the corona device. There is a countercurrent at both ends of the corona device. Momentum is axially transported. It is

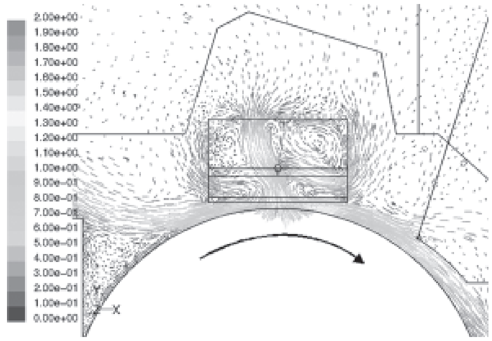

Figure 3(a). Velocity vectors in the middle plane on corona discharge in the fan-off case

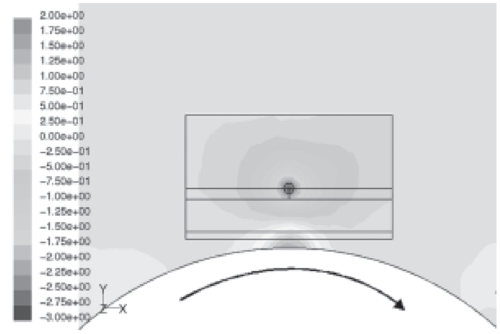

Figure 3(b). Contours of static pressure in the middle plane on corona discharge in the fan-off case

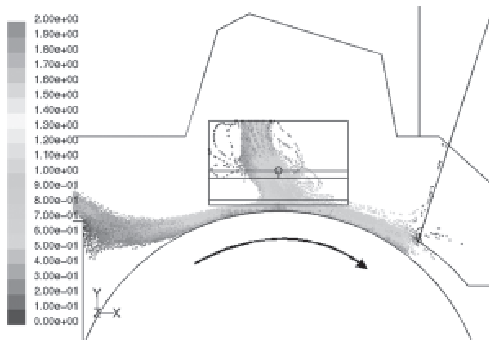

Figure 3(c). Marker particle path lines on corona discharge in the fan-off case

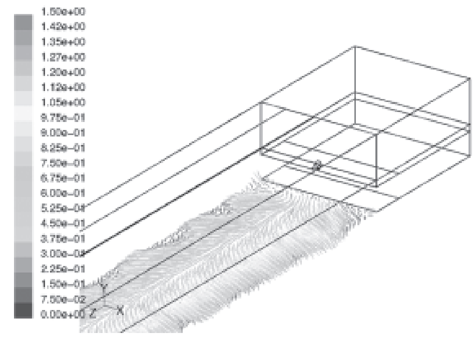

Figure 3(d). Velocity vectors at the end of the corona device in the fan-off case

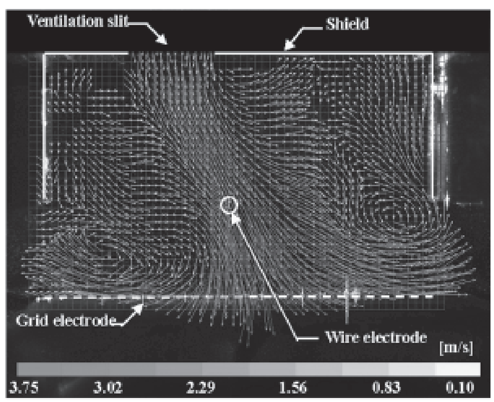

Figure 3(e). Instantaneous velocity vectors by PIV

easy to confirm these phenomena using smoke. We confirmed smoke heads for the center of the wire. Using a Pitot tube, we tried to measure the fluid field. Since the insertion of the Pitot tube exerts an influence on the flow inside corona devices, we never exactly measured the flow field in this manner.

Particle Image Velocimetry[12] (PIV) was therefore applied to measure the ionic wind around a wire electrode. We consider a simple configuration, which consists of a corona device and a photoreceptor. The observation area is 60 mm from the edge of a photoreceptor drum in the longitudinal direction. The area is covered with outer walls, which are located more than 100 mm from the wire electrode. The other experimental conditions are the same as the analysis conditions except for the rotational speed of the photoreceptor. Figure 3(e) shows instantaneous velocity vectors by PIV, with grayscale indicating velocity magnitude (m/s). The captured images were analyzed by commercial software. The photoreceptor rotates clockwise at 0.425 m/s. We found that a λ-shaped flow and vortices occur. Our numerical calculations correlate well with our experimental results. We will report the experimental setup and our findings by PIV, in detail, in a future report.

Ionic Wind Phenomenon in the Fan-on Case

In this section, we discuss the flow field in the fan-on case. We consider flow rates, velocity vectors, contours of static pressure and marker particle path lines. Table III shows flow rates for two cases. The ionic wind oc-

TABLE III. Flow Rates in the Fan-on Case

Corona discharge	Total	Ventilation slit
On	1.7180 m^3/min	0.07158 m^3/min
Off	1.7167 m^3/min	0.04077 m^3/min

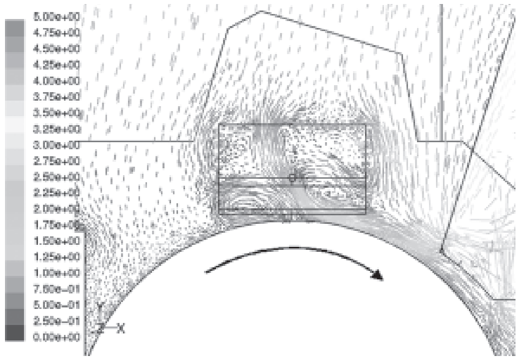

Figure 4(a). Velocity vectors in the middle plane on corona discharge in the fan-on case

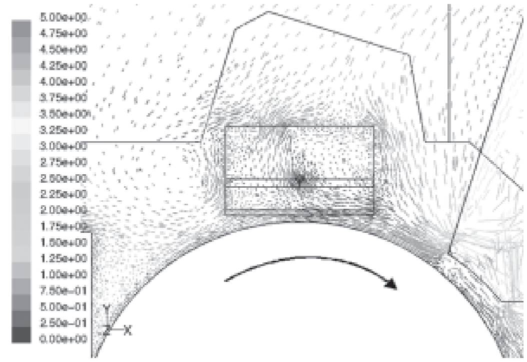

Figure 4(b). Velocity vectors in the middle plane in the fan-on case where ionic wind does not occur

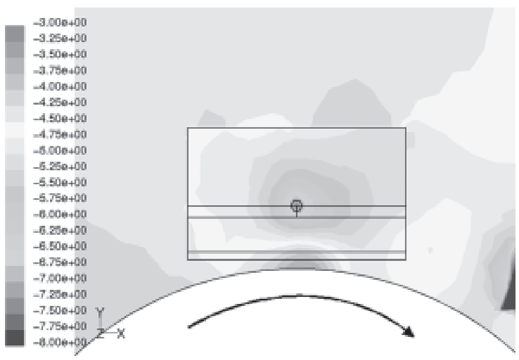

Figure 5(a). Contours of static pressure in the middle plane in the fan-on case with corona discharge

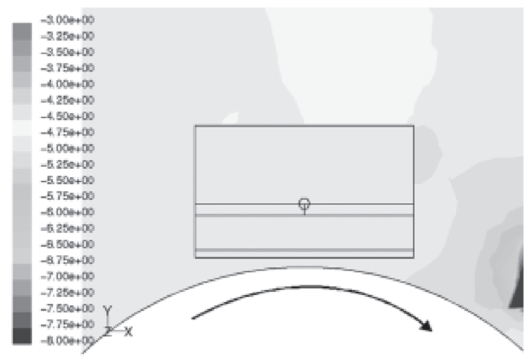

Figure 5(b). Contours of static pressure in the middle plane in the fan-on case where ionic wind does not occur

curs on corona discharge in one case; the ionic wind does not occur in other case. The flow rate of the whole system is, however, hardly changed by the influence of the ionic wind. We can conversely estimate that the mechanical impedance is 118.2 Pa.

Figures 4(a) and 4(b) show velocity vectors in the neighborhood of the corona device in the middle plane, with grayscale indicating velocity magnitude (m/s). We considered the ionic wind in Fig. 4(a), and we observed vortices in the corona device. Comparing two cases, we found that the ionic wind locally had an influence on the flow field in the neighborhood of the corona device. We similarly calculated the Reynolds number in large scale space, $R_E = 2700$, in the fan-on case. We defined a reference velocity $U = 2$ m/s and a reference length $L = 0.02$ m. It is also reasonable to assume that the flow field is laminar in the fan-on case.

Figures 5(a) and 5(b) show contours of static pressure in the middle plane, with grayscale indicating static pressure (Pa). We considered the ionic wind in Fig. 5(a). Static pressure rises at the region where the ionic wind collides with the photoreceptor. In contrast, static pressure decreases along the wire. The uniform flow field is significant in the direction from the inboard side to the outboard side for degradation of the image. We also show pressure distribution along the wire on corona discharge in Fig. 6. Static pressure falls along the wire in the range from –8.5 to –6.5 Pa. Pressure is relatively large on the inboard side. We considered that this is why the suction of the fan is relatively strong on the inboard side.

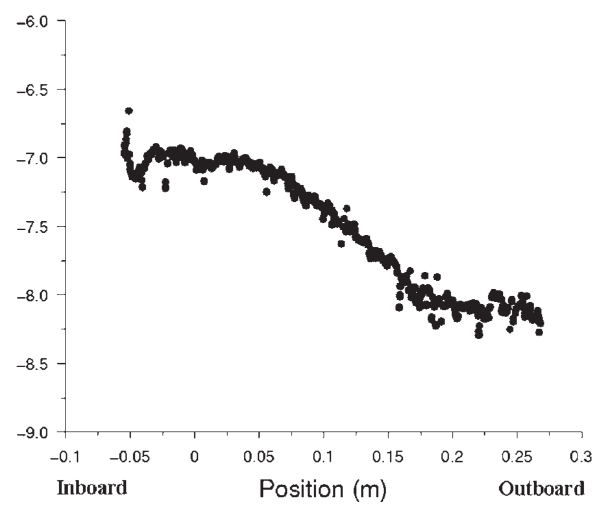

Figure 6. Pressure distribution along a wire on corona discharge

We will now discuss marker particle path lines in laminar flow. Figures 7 shows that marker particle path lines with grayscale indicating velocity magnitude (m/s) of the flow field. The λ-shaped flow appears vertically in most parts of the corona device. The flow field is strongly influenced by the rotation of the photoreceptor, espe-

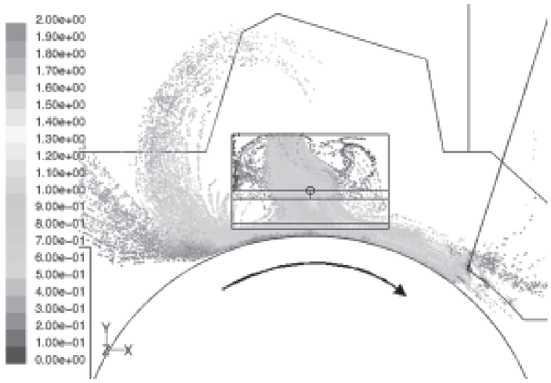

Figure 7. Marker particle path lines on corona discharge

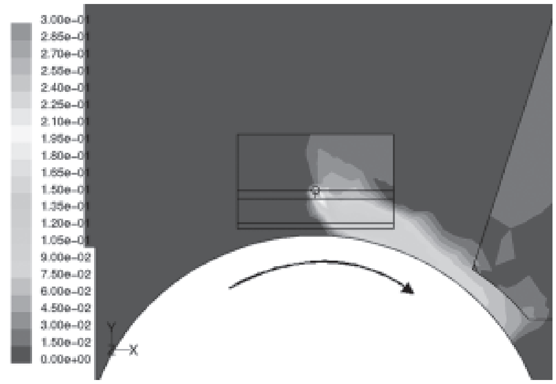

Figure 8(a). Contours of concentration of ozone in the middle plane on corona discharge in the fan-on case

cially on the upstream side. The flow field resembles the fan-off case.

Simplified Concentration Analysis

A convection-diffusion equation for species k is

$$\frac{\partial(\rho C_k)}{\partial t} + \frac{\partial(\rho u_j C_k)}{\partial x_j} = -\frac{\partial}{\partial x_j}\left(D_{k,m}\frac{\partial C_k}{\partial x_j}\right) + \dot{d}_k, \qquad (6)$$

where C_k is the local fraction of species k, $D_{k,m}$ is the mutual diffusion coefficient for species k in the mixtures and $\dot{d}_k$ is the net rate of production of species k. We consider air and thin gas as binary gas mixtures, Eq. (6) becomes

$$\frac{\partial C}{\partial t} + \frac{\partial(u_j C)}{\partial x_j} = -\frac{\partial}{\partial x_j}\left(\frac{D\,\partial C}{\rho \partial x_j}\right) + \frac{1}{\rho}\dot{d}, \qquad (7)$$

where C is the local fraction of thin gas, D is the diffusion coefficient of thin gas and $\dot{d}_k$ is the net rate of production of thin gas. Since the composition dependence of the mutual diffusion coefficient is small for binary gas mixtures, we can calculate the diffusion coefficients.[13–14] The diffusion coefficients of ozone, nitric oxide and nitric dioxide are as shown:

$$\frac{D(O_3)}{\rho} = 1.53 \times 10^{-5} m^2 / s,$$

$$\frac{D(NO)}{\rho} = 2.12 \times 10^{-5} m^2 / s,$$

$$\frac{D(NO_2)}{\rho} = 1.46 \times 10^{-5} m^2 / s.$$

For the concentration analysis, we establish the boundary condition where concentration at the outside walls is zero. We gave a constant value of 3.89×10^2 kg/m^3·s to fluid cells of the neighborhood of the wire as the source. Concentration is influenced by diffusion from the outer walls according to Fick's law in addition to exhausting by the fan. We assume that the surfaces of the photpreceptor and the inner walls are impermeable to the thin gas.

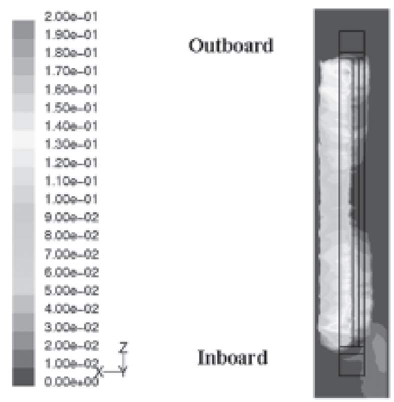

Figure 8(b). Contours of concentration of ozone on the surface of the photoreceptor on corona discharge in the fan-on case, top view

Myochin and co-workers[15] studied two-dimensional ozone concentrations. They also reported that the reduction of the quantity of ozone, the negative influence of ozone flow on a photoconductor, and improvement in image quality may be accomplished without reducing the surface potential. We used 1.53×10^{-5} m^2/s as the diffusion coefficient for ozone represents as the thin gas. Yazaki[16] observed that the ozone concentration in the corona device gradually increases with the airflow for a system having push and pull fans. FLUENT numerically predicted contours of the ozone concentration in the middle plane for our model as shown in Fig. 8(a). The concentration is dimensionless. After corona discharge, ozone must be efficiently exhausted. The efficient exhaustion of ozone will be obstructed by stagnation. We also show contours of the concentration of ozone on the surface of the photoreceptor for our model in Fig. 8(b). Ozone is distributed in a limited area on the rotating photoreceptor surface.

Summary

We have investigated the characteristic of the ionic wind. Especially, we have shown the flows field in the neighborhood of a corona device. We have discovered the following:

- The λ-shaped flow vertically appears in most parts of the corona device. This flow is strongly influenced

by the rotation of the photoreceptor on the upstream side. At the same time several vortices are induced by the λ-shaped flow in the neighborhood of the corona device.
- Our numerical calculations correlate well with our experimental results by PIV in the fan-off case.
- Static pressure rises in the region where the ionic wind collides with the photoreceptor. In contrast, static pressure decreases along the wire.
- There is a countercurrent at both ends of the corona device in the fan-off case. Momentum is axially transported.
- The ionic wind has a local influence on the flow field in the neighborhood of the corona device. However, the flow rate of the whole system is hardly changed in the fan-on case.
- The pressure falls along the wire in the range from –8.5 to –6.5 Pa in the fan-on case.

It is significant for machine design to consider control of the three-dimensional flow field. The fluid flow phenomenon is basically nonlinear and coupled. Corona devices have infinite variety; different phenomena can occur depending on the system configuration.

Recently, Computational Fluid Dynamics has advanced remarkably owing to its rapid computational development. It enables us to obtain various flow characteristics. In this article, we have shown the basic characteristics of the ionic wind. We confirm that our approach is effective in designing corona devices, and we intend to report the possibility of the application of Computational Fluid Dynamics, behavior of the ionic wind in a double corona device with push-pull ventilation, etc., in future articles.

References

1. E. M. Williams, *The Physics and Technology of Xerographic Processes*, John Wiley and Sons, New York, 1984.
2. A. Yabe, Y. Mori and K. Hijikata, EHD study of corona wind between wire and plate electrodes, *AIAA Journal* **16,** 340 (1978).
3. K. Mori, Computational fluid dynamics of dispersed mist phenomenon in a thermal ink jet printer, *J. Imaging Sci. Technol.* **47,** 250 (2003).
4. Y. Itoh, M. Yoshizawa, T. Tsuzuki, and M. Sugawara, Numerical analysis of the fluid field near the corona wire due to the corona discharge (The vortex formation and the fluid force on the wire), *Trans. Jap. Soc. Mech. Eng.* (C). **64,** 4115 (1998), (In Japanese).
5. L. Léger, E. Moreau and G. G. Touchard, Effect of a DC corona electrical discharge on the airflow along a flat plate, *IEEE Trans. Ind. Appl.* **38,** 1478(2002).
6. T. Yamamoto, M. Okuda and M. Okubo, Three-dimensional ionic wind and electrohydrodynamics of tuft/point corona electrostatic precipitator, *IEEE Trans. Ind. Appl.* **39,** 1602(2003).
7. K. Nashimoto, The Effect of electrode materials on O_3 and NO_x emissions by corona discharge, *J. Imaging Sci.* 32, 205 (1988).
8. Y. Hoshino and H. Hayashi, Effect of airflow and Isopar™ vapor on corona discharge, *J. Imaging Sci. Technol.* **47,** 13 (2003).
9. H. Okamoto and K. Mori, Computational fluid dynamic analysis of ionic wind in corona devices, *Proc. IIP/ISPS Joint MIPE '03,* JSME, Tokyo, Japan, 2003, p. 319.
10. M. P. Sarma and W. Janischewskyj, DC corona on smooth conductors in air, *Proc. IEEE* **116,** 161 (1969).
11. Fluent Inc., FLUENT 6.0 UDF Manual, Fluent Inc.,Lebanon, NH, 2001.
12. N. Hirooka, Y. Ono, K. Mori, and N. Nakayama, PIV measurements of airflow and ink mist motion around ink jet nozzles, *Proc. NIP19: International Conference on Digital Printing Technologies*, IS&T, Springfield, VA, 2003, p. 284.
13. B. E. Poling, J. M. Prausnitz and J. P. O'Connel, *The Properties of Gases and Liquids* 5th ed., McGraw-Hill International Editions, 2001.
14. T. H. Chung, M. Ajlan, L.L. Lee and K. E. Starling, *Ind. Eng. Chem. Res.* **27,** 671 (1988).
15. H. Myochin, Y. Inoue and J. Okuno, Development of corona charger for the reduction of the bad influence of ozone on a photoconductor, *Soc. J. Electrophotography.* **31,** 53 (1992), (In Japanese).
16. N. Yazaki, Air Flow Design of the Color Copiers for Environmental, *Ricoh Technical Report.* **25,** 98 (1999), (In Japanese).